10

Radiation Safety

Yoshihiro Asano
Safety Design Group, SPring-8/RIKEN, Japan

1. Introduction

Radiation safety is one of the most important issues for free electron laser [FEL] facilities and the users. Many FEL facilities are under operation worldwide, and their number is growing. The wave length of FEL ranges from a few millimeters to about 0.5 nm, and the electron energy is from a few MeV to about 20 GeV. Furthermore, various kinds of electron accelerator types are constructed for FEL facilities, such as Linac, and storage rings. In this chapter, radiation means ionizing radiation, excluding non-ionizing radiation. Radiation sources in relation to FEL facilities are γ (X) ray (high energy photons), electron, neutron due to thephoto-nuclear reaction, and muons. Activation is another important problem for high-energy accelerators.

An radiation safety system depends strongly on the machine and the energy. Based on ALARA* (As Low As Reasonably Achievable) principle, therefore, the safety system must be constructed to be better suited for the machine as much as possible. Radiation safety for FEL mainly consists of, (1) the beam containment system, including shield, (2) the access control system, and (3) the radiation monitoring system. These systems are linked organically by on interlock system to prevent the hazardous conditions. There are fundamentally no differences between FEL facilities and high-energy electron accelerators, especially synchrotron radiation facilities.

2. Safety system

2.1 Outline of basic quantities for radiation protection

Basic quantities for radiation safety are the absorbed dose, D, and effective dose, E. The absorbed dose, D, is a physical quantity, and the quotient of $d\bar{\varepsilon}$ by dm is as the follows:

$$D = d\bar{\varepsilon} / dm , \tag{1}$$

where $d\bar{\varepsilon}$ is the mean energy imparted to a tissue organ of mass dm for radiation safety. The unit is Joule・kg^{-1} and the special name for the unit is Gray (Gy) (Another unit is erg・g^{-1} and the unit of rad (1rad=10^{-2}Gy)). The effective dose E is a quantity for radiation protection control, and the special name for the unit is Sievert (Sv). (Another unit is rem (1 rem =10^{-2}

*ALARP: "As Low As Reasonably Practicable", principle is used in UK

Sv)). Since the biological effectiveness of radiation exposure is different for various types of radiation, irradiation conditions, and irradiated tissues or organs, the effective dose, E, is the unified quantity to discuss and utilize for radiation protection against the different biological effectiveness. The effective dose, E, is calculated in three steps, as follows (1): (1) The mean absorbed doses, D_T, in a specified tissue or organ T of the human bodies calculate in the first step as follows:

$$D_T = \frac{1}{m_T}\int_{m_T} D \cdot dm \,, \tag{2}$$

where m_T is the mass of the tissue or organ, T.

(2) The equivalent dose, H_T, which is corrected dose for different biological effectiveness due to different type of radiation, R, by using radiation weighting factor, w_R , calculates in the second step as follows,

$$H_T = \sum_R w_R \cdot D_{T,R} \,, \tag{3}$$

where w_R is given by the ICRP recommendations (2), which based on the function of linear energy transfer, LET. For neutrons, w_R is given as a function of energy, as shown in Fig.2-1. The w_R of the γ (X) ray, electron, and muon are given as 1.

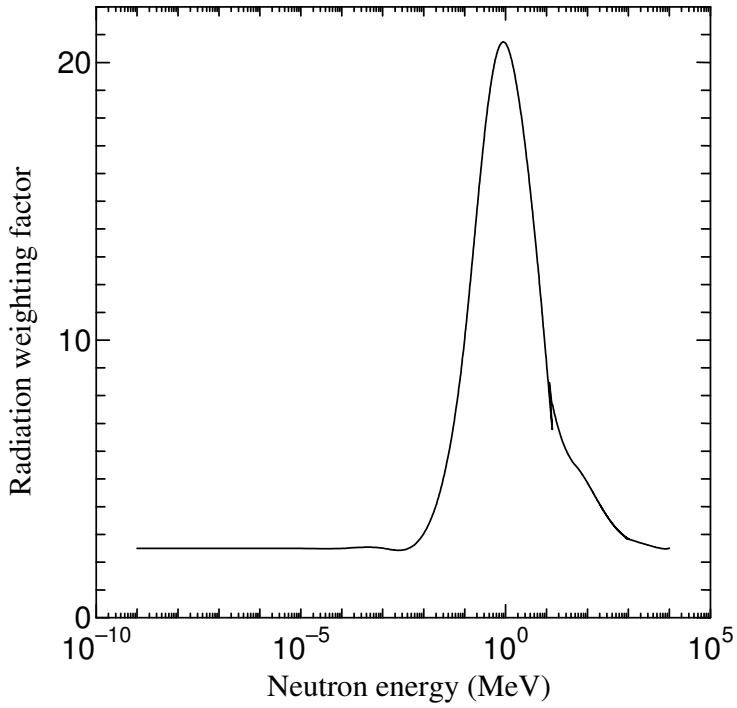

Fig. 2.1. Radiation weighting factor for neutrons.

(3) Effective dose, E, is the sum of the weighted equivalent doses in all tissues and organs of the body by using weighting factor of the tissue or organ, w_T and an anthropomorphic phantom, as follows:

$$E = \sum_T w_T \cdot H_T \ , \tag{4}$$

where w_T is given by the ICRP recommendations (2) for each of 14 organs and others as given in Table 2-1.

As mentioned above, the effective dose, E, is not easily calculated,so that the tables and figures of the effective doses, E, are presented for the unit fluence of the typical irradiation conditions as a function of the radiation energy (3,4). In order to measure and simplify the doses, operational doses, such as the ambient dose equivalent, directional dose equivalent, and personal dose equivalent are defined (5) for practical use, and these doses are fundamentally conservative in comparison with the effective dose, E.

Tissue or organ	Tissue weighting factor w_T
Bone marrow (red)	0.12
Colon	0.12
Lung	0.12
Stomach	0.12
Breast	0.12
Gonads	0.08
Bladder	0.04
Liver	0.04
Oesophagus	0.04
Thyroid	0.04
Skin	0.01
Bone surface	0.01
Brain	0.01
Salivary glands	0.01
Remainders*	0.12

*Remainders: adipose tissue, adrenals, connective tissue, extrathoracic, airways, gall bladder, heart wall, kidney, lymphatic nodes, muscle, pancreas, prostate, small intestine wall, spleen, thymus, and uterus/cervix

Table 2.1. Tissue weighting factors (2)

2.2 Outline of dose limitation system

Based on the fundamental rules of justification and optimization, dose limitation systems are performed under the achievement of consensus. The main dose limitations that International Commission on Radiation Protection (ICRP) recommends are listed in Table 2-2.

Radiation worker	100mSv/5y, 50mSv in any year, 20mSv/y averaged 5y
	H_T;150mSv/y (lens eye), 500mSv/y(skin, legs, hands),
Radiation worker(pregnant)	H_T ; 1mSv/ embryo/fetus,
Public	E;1mSv/y
	H_T ; 15mSv/y (lens eye), 50mSv/y(skin),

Table 2.2. Main ICRP recommendations for dose limitation. (2)

Based on the ICRP recommendations, each country or facility employs the design criteria of dose limitation. For example, the design criteria of the dose limitation at SPring-8 are 8 μSv/h (40hours for 1 week radiological worker occupancy), 2.5 μSv/h, and 100 μSv/y, for a radiation-controlled area, the boundary of the controlled area, and the site boundary of SPring-8, respectively (5). At Stanford national linear accelerator center, SLAC, the design criteria are 10mSv/y (5mSv for 2000h radiological worker occupancy), 1mSv/y (0.5mSv for 2000h non-radiological worker occupancy) for normal operation, 4mSv/h for miss steering conditions, 30mSv/event for system failure (6).

2.3 Radiation sources

Radiation corresponding to the safety at FEL facilities is (1) X-rays produced by synchrotron radiation, (2) X-rays due to high density of lasers, (3) γ -rays due to high energy electron-beam loss, including gas bremsstrahlung, (4) neutrons due to photo-nuclear reactions, and (5) muons. The importance of each type of radiation for safety strongly depends on the energy of the electron machine and the power of the laser, as described below:

1. A free-electron laser is produced by undulators with oscillation and the coherency of the synchrotron radiation so that the spontaneous emission light of the undulator is also produced. Generally, the spontaneous emission light is more important for safety because of strong penetration of high-energy photons (7).
2. The interaction of a high-intensity laser with matter generates plasma and associated produced high-energy electrons and ions. These high-energy electrons interact with ions in the target and induce bremsstrahlung X-rays (8). X-rays will be produced when the laser is focused on a target at peak intensities of over 10^{12} W/cm^2 (9), and neutrons and protons may be produced at the peak intensities over 10^{19} W/cm^2 (10)
3. Interactions of high-energy electrons with matter, such as electron beam transport pipe or shield materials produce an electro-magnetic shower and high-energy γ rays (11). In this case, the energy of the photons distribute up to the maximum accelerated electron energy. Interactions of high-energy electrons with residual gas molecules within the electron beam transport pipe of undulators produce high-energy γ rays, so called “gas bremsstrahlung” with high directivity in special cases (12).
4. The interactions of γ rays with the energy of over about 10 MeV with thick materials produce neutrons due to the nuclear reactions of the giant resonance, quasi-deutron and photo-pion reaction process.
5. Interactions of high-energy γ-rays with thick materials also produce muons. In this process, because the threshold energy of the muon production is 211 MeV, the muons must care at high-energy machines.

2.4 Radiation monitoring

Radiation monitoring is classified into two categories: one for personnel monitoring and the other for area monitoring. Because the personnel monitoring is to measure and confirm individually the personal dose, badge types are employed to equip on radiation workers. Now, OSLs (Optical Stimulate Luminescence, TLDs (Thermo Luminescence Detectors), film badges (13), and Glass dosimeters (14), etc are used to measure the γ (X)ray dose. For a dose due to high energy neutrons, CR-39 neutron track detectors are employed, mainly.

The area monitoring is to clarify the circumstances of the radiation fields at the facility so that the monitors will be assigned at the position where the dose will be increased in comparison with the dose limitation. Ionization chambers are usually used for γ (X)ray area monitors. Plastic scintillation counters are employed at some facilities (15) to measure pulsed radiations. For neutron monitoring, Helium-3 or BF_3 proportional counters with moderators are used. Some facilities employ superheated drop detectors (bubble detectors) [16].

2.5 Safety interlock system

A radiation safety interlock system is one of the key issues for accelerator facilities, including FELs. The safety interlock system must be constructed with high reliability and fail-safe system, however, the system depends strongly on each facility design and the safety philosophy. The conceptual main frame of the safety interlock system is shown in Fig.2-2. The equipment of the interlock system is linked fundamentally to a PLC (Programmable Logic Controller) using hard wires to stop the machine operation infallibly. Multiplex systems are often employed such as a door keep system, emergency button and a beam shutter system. It depends on the level of the importance or hazardous and the credibility of the system to construct to the multiplex system.

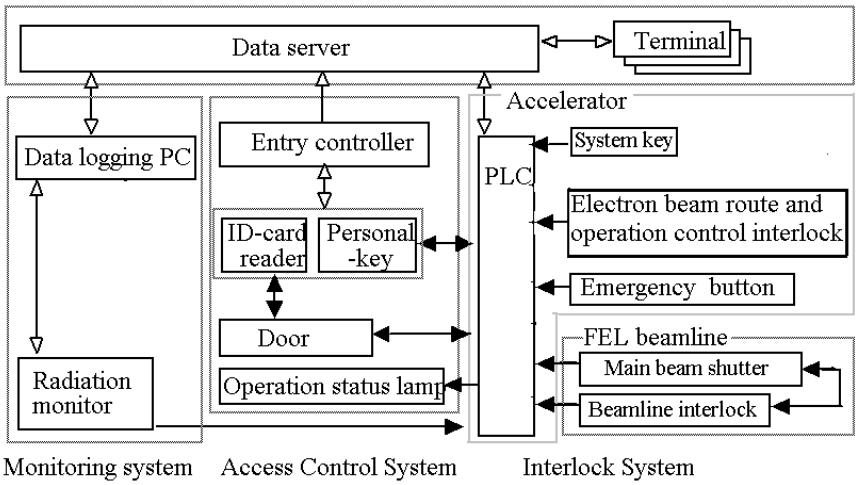

Fig. 2.2. Conceptual main framework of the safety interlock system (PLC: Programmable Logic Controller, Black full arrows mean to connect interlock system)

3. Shielding design

There are mainly two methods for shielding design. One is to use Monte Carlo simulation codes; the other is to use analytical and empirical method. Normally, close checks between Monte Carlo simulations and the results of empirical methods are required to confirm the design.

3.1 Monte Carlo code

The Monte Carlo codes can simulate radiation transport with complicated geometry. Typical Monte Carlo codes to perform the shielding design of FEL facilities are summarized in Table 3-1. The codes have characteristic differences from each other, such as the available nuclear reaction and the maximum electron energy etc so that one must pay attention to choose the code.

Code	Type	References
EGS4 or EGS5	Electro-magnetic shower (γ ,e), exclude (γ ,n) reaction	17
Penelope	Electro-magnetic shower (γ ,e) , exclude (γ ,n) reaction	18
MCNPX	Multipurpose transport	19
MARS15	Multipurpose transport and heavy ion transport	20
FLUKA	Multipurpose transport including induced activity	21
GEANT4	Multipurpose transport including induced activity	22
PHITS	Multipurpose particle and heavy ion transport	23

Table 3.1. Monte Carlo simulation code for using the shielding design of the FEL facility

3.2 Analytical and empirical methods

3.2.1 Synchrotron radiation

The leakage dose due to synchrotron radiation spontaneous photon emission can be calculated by using the STAC8 code [24]. This code can calculate doses outside the shield material from an undulator source to the leakage dose due to scattering photons, sequentially. Doses due to FEL can be calculated by using STAC8 with the calculated FEL source spectrum by using something such as SIMPLX [25]. Generally, FEL can be neglected because of low energy-photons in comparison with the synchrotron-radiation spontaneous emission photons.

3.2.2 Plasma X-ray

Intense laser over 10^{12} W/cm^2 can produce plasma and associated X-rays. The dose can be calculated as follows [26]:

$$H_x \approx 6.0 \times (P_{ef} / R^2) \times T \qquad (T \geq 3MeV), \tag{10}$$

$$H_x \approx 2.0 \times (P_{ef} / R^2) \times T^2 \qquad (T \leq 3MeV), \tag{11}$$

$$T \approx 6.0 \times 10^{-5} \left[I\lambda^2 \right]^{1/3} \qquad (10^{12} W / cm^2 \mu m^2 < I\lambda^2 < 10^{17} W / cm^2 \mu m^2), \tag{12}$$

$$T = M_e \times (-1.0 + \sqrt{1.0 + I\lambda^2 / 1.37 \times 10^{18}} \quad (I\lambda^2 > 10^{18} W / cm^2 \mu m^2), \tag{13}$$

Here, H_x is the photon dose in Sv in the forward direction, P_{ef} is the laser energy to the electron energy conversion efficiency, R is the distance from the target to the measurement point in cm. T is the hot electron temperature in MeV. I is the laser intensity in W/cm², λ is the laser wave length in μm.

3.2.3 High energy γ ray and neutron due to electron beam loss

Radiation due to electron beam loss is an anisotropic distribution with strongly high in forward direction so that the shielding design is normally considered manner for two directions, forward and lateral directions, from the electron beam.

a. Forward direction (11)

γ-ray leakage doses can be calculated as follows:

$$H_\gamma = (P / r^2) \times 20 \times E_e^2 \times \exp(-d / \lambda_\gamma) \quad (1 < E_e < 20 MeV) \text{ (Sv/h)}, \tag{14}$$

$$H_\gamma = (P / r^2) \times 300 \times E_e \times \exp(-d / \lambda_\gamma) \quad (E_e \geq 20 MeV) \text{ (Sv/h)}, \tag{15}$$

$$H_\gamma = (P / r^2) \times 10^6 \times E_e \times \exp(-d / \lambda_\gamma) \quad (E_e \geq 1.0 GeV) \text{ (Sv/h)}. \tag{16}$$

Also the neutron leakage dose in the forward direction can calculates as follows:

$$H_{nh} = (P / r^2) \times 4.0 \times \exp(-d / \lambda_{nh}) \quad (E_e \geq 50 MeV) \text{ Sv/h)}, \tag{17}$$

$$H_{nt} = (P / r^2) \times 22.7 \times \exp(-d / \lambda_{nt}) \text{ (Sv/h)}, \tag{18}$$

Here H_γ is the γ-ray dose in Sv/h, P is the electron beam loss power in kW, r is the distance from the loss point to the measurement point in m, d is the thickness of the shielding material in cm; λ_γ, λ_{nh}, and λ_{nt} are the attenuation length of γ-rays, high-energy neutron and the giant resonance neutron, respectively. These attenuation lengths are summarized in Table 3-2. H_{nh} and H_{nt} in Sv/h mean the dose due to high-energy neutrons and the dose due to giant resonance neutrons, respectively.

Shield material	Attenuation length (cm)		
	λ_γ	λ_{nh}	λ_{nt}
Lead	2.1	66.7	23.8
Iron	4.5	58.8	18.5
Ordinary Concrete*	19.0	41.8	17.7

*Density: 2.2g/cm³

Table 3.2. Attenuation length the shield materials for the forward direction

b. Lateral direction

The neutron and γ-ray doses for the lateral direction can be calculated by using an analytical code, SHIELD11, which was developed by Stanford National Linear Accelerator Center [27]. This code can calculate the leakage dose due to beam loss, ranging from over 1 GeV to about 20 GeV electron energy.

The γ-ray doses due to electrons with an energy of less than about 20 GeV can be calculated as follows [28]:

$$H_{\gamma} = P \cdot 50 \cdot \frac{1}{r^2} \cdot \exp(-d / \lambda_{\gamma}) \qquad 50\ \text{MeV} \le \text{Ee} \le 150\ \text{MeV}\ \ (\text{Sv/h}), \tag{19}$$

$$H_{\gamma s} = 3.6 \times 10^{-14} \cdot J \cdot E_e \cdot \frac{1}{r^2} \cdot \left(\frac{133 \cdot \exp\{(-d \cos ec\phi) / \lambda_{\lambda}\}}{(1 - 0.98\cos\theta)^{1.2}} + \frac{f1 \times 0.267 \cdot \exp\{(-d \cos ec\phi) / \lambda_{\gamma}\}}{(1 - 0.72\cos\theta)^2} \right) \quad (30° < \theta < 130°)(\text{Sv/h}) \tag{20}$$

The neutron dose due to electrons with the energy of less than About 20 GeV can be calculated as follows [28]:

$$H_n = P \cdot 22.7 \cdot \frac{1}{r^2} \cdot \exp(-d / \lambda_1) \qquad (\approx 10MeV \le E_e \le 50MeV)\ \ (\text{Sv/h}), \tag{21}$$

$$H_n = 3.6 \times 10^{-14} \cdot J \cdot E_e \cdot \frac{1}{r^2} \cdot \left(\frac{f1 \cdot \exp\{(-d \cos ec\phi) / \lambda_1\}}{(1 - 0.72\cos\theta)^2} + \frac{f2 \times 10 \cdot \exp\{(-d \cos ec\phi) / \lambda_3\}}{(1 - 0.75\cos\theta)} + 3.79 \cdot Z^{0.73} \cdot \exp\{-d \cos ec\phi / \lambda_2\} \right) \quad (30° < \theta < 130°)(\text{Sv/h}) \tag{22}$$

Here, λ_{γ}, λ_1, λ_2, and λ_3 are the attenuation length of γ-rays, high-energy neutrons, giant resonance neutrons, and intermediate neutrons, as summarized in Table 3-3, respectively. J is the amount of electron beam loss in s^{-1}. f_1 and f_2 are correction factors of source reduction for high-energy and intermediate-energy neutrons [29], respectively. θ and ϕ are inclined degrees from the electron beam axis to a measurement point and the shield material, respectively. Z is the atomic number of a target.

Shield material	Density (g/cm^3)	Attenuation length (cm)			
		λ_{γ}	λ_1	λ_2	λ_3
Lead	11.3	2.1	22.7	10.0	18.3
Iron	7.8	4.3	21.3	6.8	12.4
Ordinary Concrete	2.2	18.9	54.6	13.7	25.0

λ_{γ}, photon; λ_1:, high energy neutron; λ_2, giant resonance neutron; λ_3, intermediate energy neutron

Table 3.3. Attenuation length for the lateral direction

3.2.4 Gas bremsstrahlung and associated neutrons

The combination of a long straight section for undulators and high-energy electrons generates gas bremsstrahlung by interactions of the accelerated electrons with residual gas molecules in a vacuum chamber. The dose due to gas bremsstrahlung is in proportion to the current of the electrons, the pressure of the residual gas molecules, and the length of the straight section, as follows [30]:

$$D = 2.5 \times 10^{-27} \cdot \left[\frac{E_e}{m_0 c^2} \right] \cdot \frac{L}{d(L+d)} \cdot I \cdot \frac{P}{P_0}, \tag{23}$$

where D is the maximum dose rate due to gas bremsstrahlung in Gy/h, m_0c^2 is electron rest mass (0.511MeV), E_e is the electron energy in MeV, L is the length of the straight section in m, and d is the distance from end of the straight section in m. I is the current of electrons in $e^- \cdot s^{-1}$, P is the pressure of the straight section in Pa, and P_0 is 1.33×10^{-7} Pa. Photo-neutrons are produced when gas bremsstrahlung photons have a sufficiently high energy. In this case, the dose can be estimated by using Liu's data [31]. The doses due to gas bremsstrahlung and associated neutrons are negligibly small at almost the FEL facilities.

3.2.5 Muon

Muons are produced by high-energy photons in the Colomb field of the target directly and the decay products of photo-produced π and K mesons. The dose due to muons can be used to calculate as follows [11]:

$$H_{\mu} = \frac{25}{25 + X/X_0} \times \frac{X(\mathrm{E_e})\text{-}X}{X(\mathrm{E_e})} \times H_0 \qquad (\mathrm{X(Ee) > X}) \ \ (\mathrm{Sv/h}), \tag{24}$$

$$H_u = 0.0 \qquad (X(E_e) \le X), \tag{25}$$

$$H_0 = 8.0 \times 10^{-15} \cdot J \cdot E_e / r^2 \ \ (\mathrm{Sv/h}) \tag{26}$$

where X is the thickness of the shield material, and X_0 is the radiation length of the shield material and summarized in Table 3-4. $X(E_e)$ is the maximum possible muon range of the shield material, as summarized in Table 3-5 for various energies. The muon dose is negligibly small at facilities with an electron energy of less than about 10 GeV.

Shield material	Radiation length		Density
	(g/cm^2)	(cm)	(g/cm^3)
Lead	6.4	0.6	11.3
Iron	13.8	1.8	7.8
Ordinary Concrete	25.7	11.7	2.2

Table 3.4. Radiation length of shield materials

Shield materials	Maximum Range (g/cm²)				density
	0.3GeV	1GeV	7GeV	10GeV	(g/cm³)
Lead	233	809	4857	6696	11.3
Iron	176	629	3968	5522	7.8
Ordinary Concrete	144	526	3324	4624	2.2

Table 3.5. Maximum possible muon range

3.2.6 Maze streaming

An maze is usually constructed at the shield tunnel of accelerators for entryways. The leakage dose outside the maze (see next section) can be calculated as follows.

For the γ -ray dose attenuation ratio of the labyrinths, g_i [32] is

$$g_1 = 0.22 \times (d + L_1)^{-3.0}, \tag{27}$$

$$g_i = 0.26 \times (d + L_i)^{-2.6} \qquad (i = 2,3,*,*,*), \tag{28}$$

and for neutrons [33],

$$n_i = 2 \times \frac{\exp(-L_i / 0.45) + 0.022A^{1.8} \cdot \exp(-L_i / 2.35)}{1 + 0.022A^{1.8}} \qquad (i = 1,2,3,*,*,*). \tag{29}$$

Here, L_i is the length of the i^{th} labyrinth in m, d is the half width of the maze in m, and A is the cross section of the access in m². For the last labyrinth, the factor 2 in formula (29) is ignored.

3.3 Induced activity

High-energy electrons of about over 10 MeV (depending on the material, for example, over about 1.68 MeV for Beryllium) can produce radioactive materials so that high-energy high-power machine must take care the induced activities within the machine components, air, cooling water, and shield materials including concretes. The induced activity produced by photo-nuclear reactions can be estimated by using the saturation activity and the electron beam loss power of the machine [11]. For example, the activity in air derives as follows:

3.3.1 Photo-nuclear reaction

$$S_A = \lambda \cdot A_{AS} \cdot P \cdot X_m \cdot F_1, \tag{30}$$

$$A(t) = \frac{S_A}{\lambda}\{1 - \exp(-\lambda \cdot T)\} \cdot \exp(-\lambda \cdot t), \tag{31}$$

where S_A is the production rate (GBq・h^{-1}),

A_{AS}; the saturation activity (GBq・kW^{-1}・m^{-1}),
P; the electron beam loss power (kW),
X_m; the photon traversable distance within air (m),
λ; the decay constant (h^{-1}),

A(t); the activity after t hours from the shutdown (GBq),
T; the irradiation time (h),
t; the time after the shutdown (h), and
F_1; the ratio of the contribution of electron beam loss to induced activity.

3.3.2 Neutron absorption (dominant nuclei; Argon-41)

$$S_A = \lambda \cdot 10^{-24} \cdot \sigma \cdot N \cdot Y \cdot e \cdot X_{cm} \cdot F_1 \cdot 10^{-9} \tag{32}$$

Here σ is the neutron absorption cross section (cm^2; Ar=0.64 b),
N; the number of atoms (cm^{-3}: ^{40}Ar=2.3x$10^{17}cm^{-3}$),
Y; the neutron yield per electron (neutrons/electrons),
Y≈2.4x10^{-3} (Ee-0.2) Ee: electron energy (GeV),
e; the electron loss rate (s^{-1}), and
X_{cm}; the neutron traversable distance within air(cm).

The air activity concentration under the operation of the ventilation system is described as follows:

$$Q\frac{dC_i}{dT} = S_{Ai} - \lambda_i \cdot Q \cdot C_i - q \cdot C_i \,, \tag{33}$$

where Q ; is the volume of air (m^3),
S_{Ai}; the production rate of i nuclei (GBq・h^{-1}),
λ_i ; the decay constant of I nuclei (h^{-1}),
C_i ; the activity concentration of i nuclei (GBq・m^{-3}), and
q ; the air volume of ventilation (m^3・h^{-1}).

Thus, the activity concentration of nuclei indicates the following:

$$C_i = \frac{S_{Ai} \big/ Q}{\lambda_i + q/Q} \cdot \left[1 - \exp\left\{-(\lambda_i + q/Q) \cdot T\right\}\right] \tag{34}$$

The saturation activities are summarized in reference (11). The important nuclei of air and water-induced activity are (^3H, ^7Be, ^{11}C, ^{13}N, ^{15}O, ^{16}N, ^{38}Cl, ^{39}Cl, ^{41}Ar), and (^{14}O, ^{15}O, ^{13}N, ^{11}C, ^{10}C, ^7Be, ^3H), respectively.

4. Radiation safety at SCSS prototype FEL facility

The SPring-8 Compact Self Amplification of Spontaneous Emission Source (SCSS) prototype FEL facility (34) has been employed to analyze practical cases of the radiation condition in comparison with the design. The SCSS prototype FEL facility was constructed in 2005 to demonstrate the feasibility of an X-ray FEL based on three new technologies, one for a low-emittance thermionic gun, one for C-band accelerators of up to 250 MeV and 30nC/s, and the other for in-vacuum type undulators. The shortest wave length of this 60 m SCSS prototype system is 49nm. Continuous lasing has been successfully performed, as shown in Fig. 4-1, and photo 4-1.

Photo 4.1. SCSS prototype FEL facility (view from the gun to the dump)

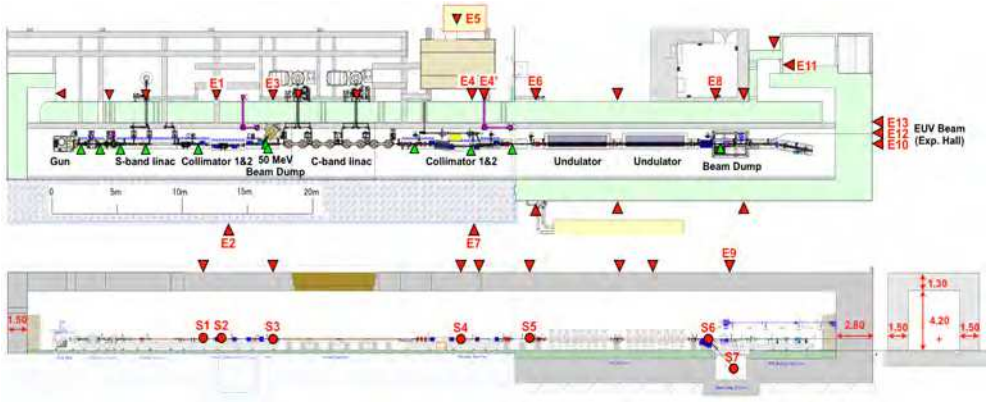

Fig. 4.1. Layout of the SCSS prototype accelerator (up, top view; down, side view;▲, leakage dose measurement & estimation points;▲, CT(Current Transformer);●, beam loss point).

The SCSS prototype has two beam dumps (one for 50 MeV electrons and the other for 250 MeV electrons), two bunch compressors with local shields, and two in-vacuum type undulators, as shown in Fig. 1. The two dumps are double-cylindrical structures with graphite for the inner cylinder and iron for the outer cylinder to reduce the production of photo-neutrons. The 250 MeV dump was constructed with an inclination angle of 45 degrees, and was embedded underground. The beam-loss distributions were measured by using subtractions of the current transformers (CT) output. The CTs are installed upstream of the dumps, the undulators, and the bunch compressors, as indicated in Fig. 4-1. The FEL light beamline including the SCSS prototype should be constructed in the forward direction of the accelerated electron beam and electron beam dump. It is thus important to prevent high-energy radiation due to electron beam loss in designing the light beamline. For the SCSS prototype, the offset between the electron beam axis and the light beamline at the end of the shield tunnel wall and the distance from the scatterer (mirror) were designed at to be

40cm and 4.5 m, respectively. The thicknesses of the shield tunnel of the SCSS prototype are ordinary concrete of 1.5 m in the lateral direction, 2.8 m in the forward direction, 1.3 m for the roof.

Two area monitors are set up outside of the shield tunnel near the downstream collimator and the beam dump. The access control systems with personal keys are installed at the two entrances. These are linked to a safety interlock system.

4.1 Shielding design

The shielding design of the SCSS prototype was achieved by using analytical methods and the FLUKA Monte Carlo code [35]. The leakage dose distributions outside the shield tunnel strongly depend on the electron beam-loss distribution. It is thus important to estimate the beam loss exactly, which is the first step of shielding design. The measurement results of the electron beam-loss distributions during lasing (user time) using CTs are shown in Fig.4.1., including typical cases of the beam tuning operation and laser-seeding experiments [36]. As shown in the figure, the beam losses occurred up to the first collimators (bunch compressor section) for all cases. During the user time, the electron beam loss is very low at the undulator section. On the other hand, the beam loss shows higher loss rates up to about 5 % in the undulator section during beam tuning and seeding experiments. Table 4-1 summarizes the measurement data and the estimated values for the shielding design. The design values were decided based on the analyses of the beam diagnoses and discussions between radiation safety physicists and accelerator physicists. These data show good agreement.

Source No.	Source Position	Beam loss Assumption（%）	Beam loss measurements (User time、%）
S1	At any points from gun to upstream collimator	15	~75
S2	Collimator(upstream)	60	
S3	Beam dump (50MeV）	(100)	
S4	Collimator(downstream)	4	~3
S5	At any point from down stream collimator to dump bending magnet	1	
S6	Dump bending magnet	1	
S7	Beam dump(250MeV)	19(100)	~22

Table 4.1. Electron beam-loss distribution at SCSS (design and measurements; source No.S1 through S7 are indicated in Fig. 4.1.)

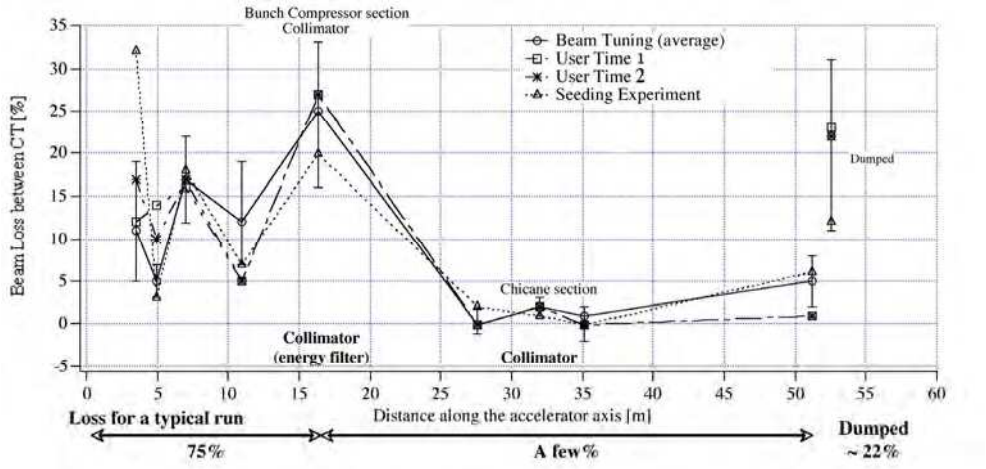

Fig. 4.2. Measurement results of the electron beam loss during three modes with 250 MeV operation.

Typical results of calculations using the analytical methods are indicated in Table 4.2. In these calculations, source reduction factors, f_1 and f_2 for 250 MeV electrons are set to be 0.09 and 0.22, respectively.

Estimate Point	Source Point	J (e/s)	Ee (GeV)	r (m)	Shield Thickness (cm)		Radiation	Dose (μSv/h)	Total dose (μSv/h)	Formula No.
E4	S4	7.5×10^{9}	0.25	3.2	O.C.	150	γ (X)	0.056	0.11	20
					Fe	8	N	0.053		22
E8	S6	1.9×10^{9}	0.25	3.2	O.C.	150	γ (X)	0.082	0.24	20
							N	0.020		22
	S7	1.9×10^{11}	0.25	3.2	O.C.	240*	γ (X)	0.016		20
					Fe	25	N	0.12		22
E10	S6	1.9×10^{9}	0.25	12	O.C.	280	γ (X)	0.19	0.19	15
							N	0.0026		17,18
	S7	1.9×10^{11}	0.25	10	O.C.	396*	γ (X)	9.0×10^{-5}		20
					Fe	25	N	6.9×10^{-4}		22

*Effective thickness

(Estimation points and source points indicate in Fig.4-1)

Table 4.2. Shielding design calculations using analytically empirical methods, for example.

SCSS prototype has two entrances as shown in Fig.4.1. Figure 4.3 shows the simulation results of the neutron dose distributions at two entrances due to electron injection into the dumps (A, electron energy of 50 MeV and source points S3; B, electron energy of 250 MeV and Source point S7) by using FULKA.

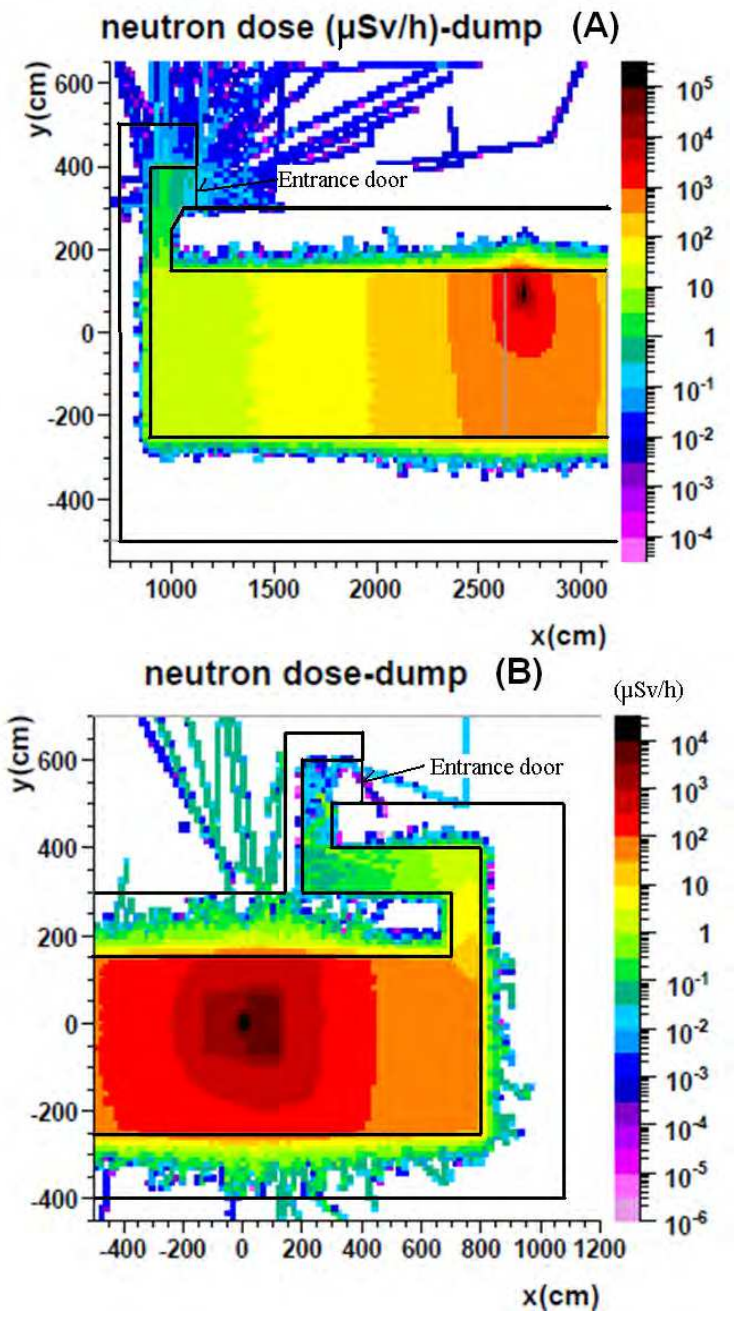

(A: 50 MeV dump(S3), B:250MeV dump(S7))

Fig. 4.3. Neutron dose distribution at the entrance of the shield tunnel of the SCSS prototype.

4.2 Dose measurements

To compare the results of the calculations, the dose distributions around the accelerator were measured in relation to the beam losses by using Gafchromic films and LiF thermo luminescent dosimeters. Andersson-Braun type rem counters and ion Chambers were used for measurements outside of the shield tunnel. Figure 4-4 shows, for example, the gamma-ray dose rate at the exit of the FEL beam from the tunnel (inner side of E12 as indicated in Fig.4-1). In Fig.4-4, the doses are normalized with the total electron charge measured at the first CT monitor. Figure 4-5 shows the dose rate in Fig. 4-4 as a function of the electron beam-loss rate at the undulator section. In this case, the doses are linearly proportional to the amount beam loss at the undulator section, and the slop is about 0.6 mGy/mC percent of the beam-loss rate.

The gamma and neutron doses outside the shield tunnel near the FEL beam transport line, as indicated by E10, E12 and E13 in Fig. 4.1 are lower than the detection level. At the SCSS, the maximum leakage dose outside the shield tunnel was about 2.0 μSv/h of the gamma rays (controlled area) for 50 MeV operation, and 0.5 μSv/h of gamma rays and 0.15 μSv/h of the neutrons (non-controlled area) for 250 MeV operation. The synchrotron radiation of the spontaneous emission light and FEL cannot penetrate the beam-transport pipe because of low energy. These leakage doses agree reasonably well with the calculations.

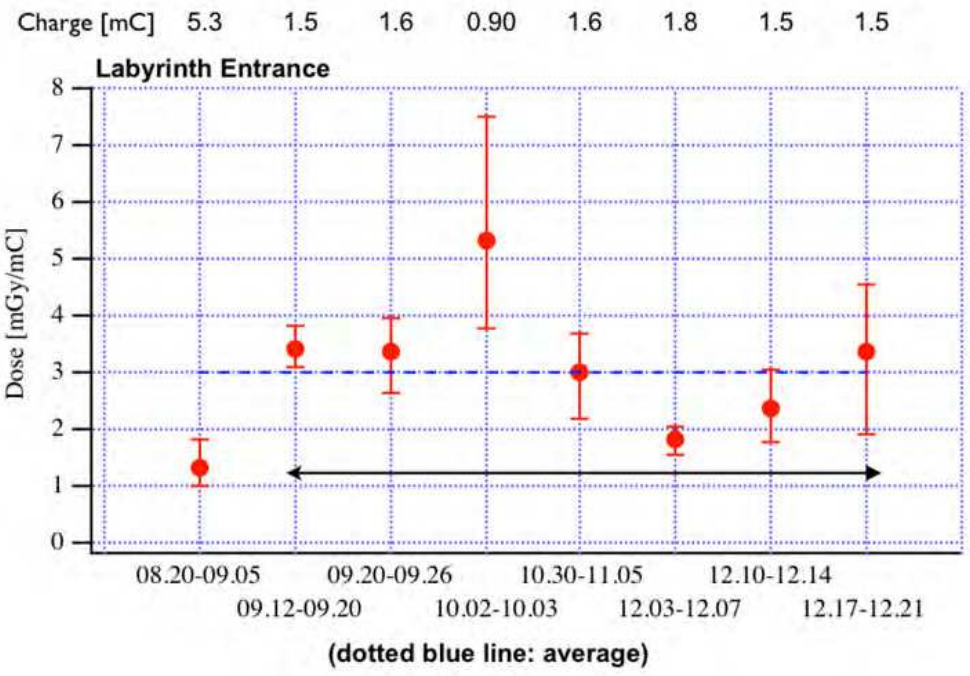

Fig. 4.4. Gamma-ray dose at the exit of the FEL beam from the tunnel (inner side of E12 as indicated Fig. 4.1.). The dose is normalized by the total electron charge at the first CT.

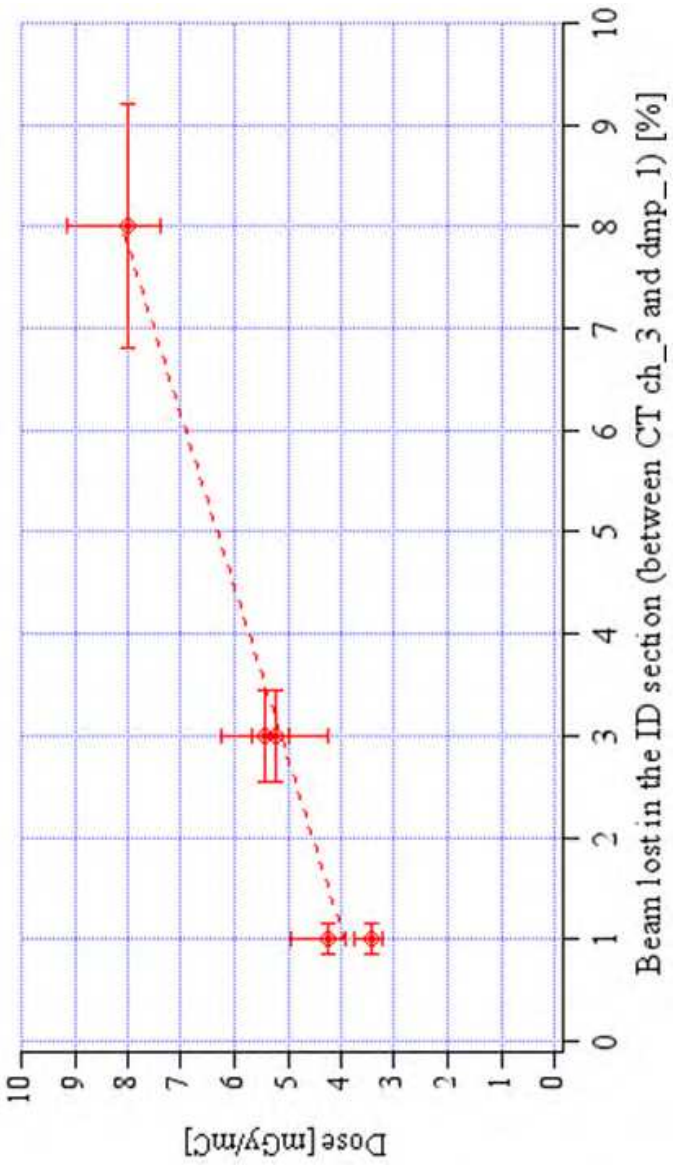

Fig. 4.5. Gamma-ray dose distribution at the FEL exit within the shield tunnel as a function of the ratio of the beam loss in the undulator section (doses are normalized by the total charge at the first CT)

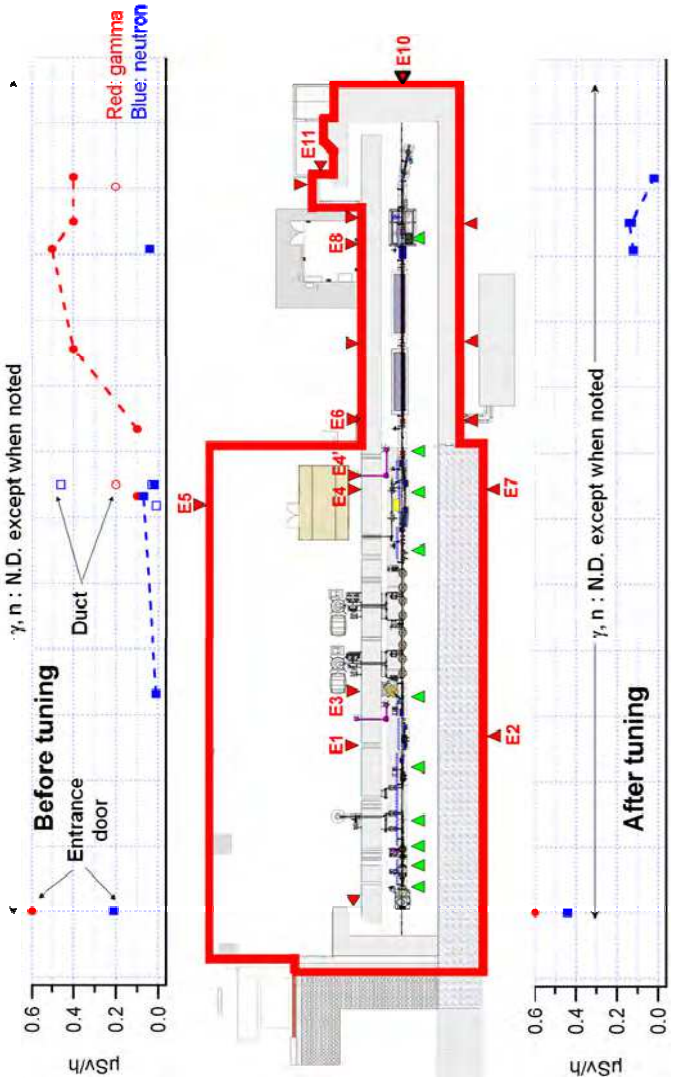

Fig. 4.6. Measurement results of the dose distribution outside the shield tunnel (250MeV operation). The red line indicates the boundary of the radiation controlled area.

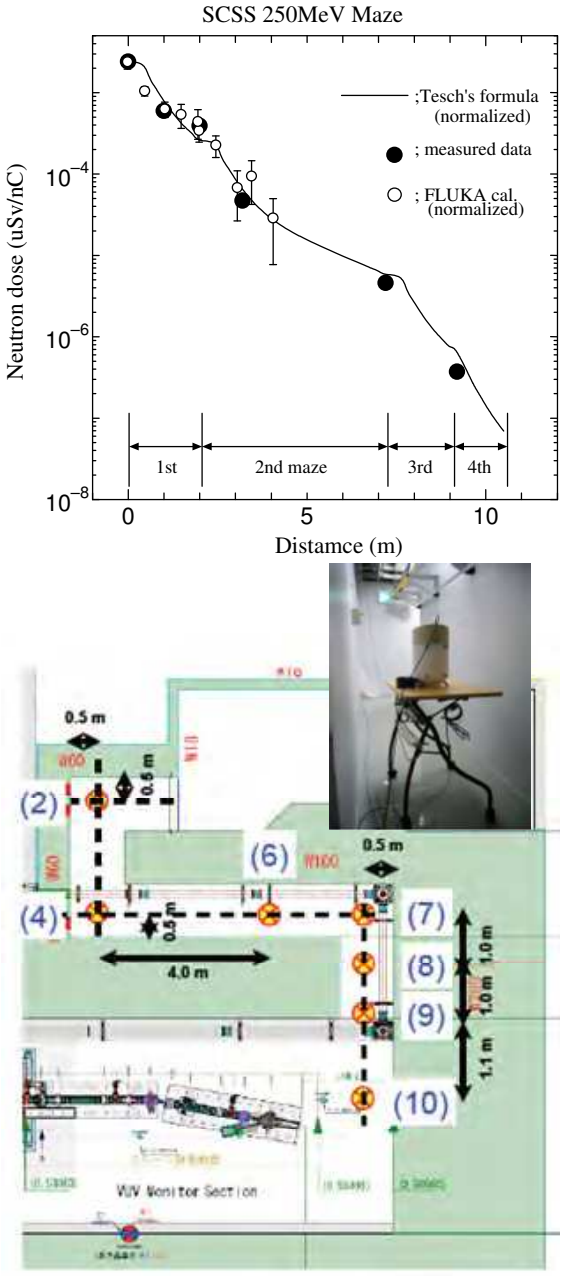

Fig. 4.7. (A) Neutron dose distribution within the maze in comparison with the calculation results of the Tesch' formula and FLUKA. (B) Neutron measurement points within the downstream maze including the photo of the Andersson Braun-type rem counter.

Figure 4.6 shows the typical dose distributions outside the shield tunnel before (beam tuning) and after (user time) the tuning operation. In Fig. 4.6, E1 through E11 are the measurement points, as shown in Fig. 4.1, and E1 through E5, except E2, are in the radiation controlled area, and others are at the boundary of the controlled area. In these cases, the characteristics of the dose distribution due to beam tuning are higher gamma doses near the undulators and 250 MeV dump (near E8) in comparison with that after the beam tuning. On the other hand, the neutron dose at the entrance door and near the 250 MeV dump are higher than that before the beam tuning. The higher neutron dose at the entrance door after the beam tuning seems to be due to harder tuning in comparison with before beam tuning at the first stage of acceleration. At E4 and E5 near the second (last) collimator, doses before beam tuning are higher than that after the beam tuning. These phenomena agree with the electrons accelerating to the last collimators without tuning and being scraped out by it. The gamma-ray dose at the upstream entrance door is due to scattered X-rays from the thermionic gun of 500 keV high voltage with over 1A current and the cut of the corner of the maze to carry on some instruments easily, as shown in Fig. 4.3(A).

The measured data of neutron doses within the downstream maze are shown in Fig.4.7(A), including the calculation results using Tesch's formula (29) and the FLUKA Monte Carlo code. Fig. 4.7(B) shows the measurement points in the Maze. In the figure, the neutron doses are normalized with the charge of electrons injected into the dump. Both calculations are normalized at the maze entrance in the shield tunnel (0 m in Fig.4.7, and (9) in Fig 4.7 (B)). Both calculations, Tesch's formula and FLUKA, agree well with the measurement results so that Tesch's formula can reproduce the photo-neutron dose distribution within the maze due to the 250 MeV electrons.

According to planning and expectation, the dose at the light beamline outside the shield tunnel (E12 in Fig. 4.1) was under the detection level because of a sufficient offset of 40 cm between the electron beam axis and the FEL light beam line, and the low energy of the spontaneous emission light including FEL. There are no significant induced activities, except for short life nuclei, at the machine components until now.

5. Summary

Radiation safety systems for Free Electron Laser facilities are overviewed. Practical cases are presented using the SCSS prototype facility in comparison with the shielding design and the measurement data of leakage doses. Three dose limits must be considered normally, one for radiological worker occupancy, including miss-steering condition, one for the boundary of the radiation controlled area, and the other for the site boundary. The shielding is design therefore required to be lower than the three criteria sufficiently, and the criterion of the site boundary is more sever in many cases. In addition, the shielding design and the radiation safety system depend on the electron beam loss scenario directly, so that intense scrutiny of the beam-loss scenario is necessary, and close communications with the radiation safety physicists and the accelerator physicists is important. Others are thermal and laser problems. Both problems will be become more significant with increasing the power of the free electron laser.

6. References

[1] ICRP publ. 60 " Recommendations of the International Commission on Radiological Protection, adopted by the commission on Nov. 1990". Annuals of ICRP, Permagon Press Oxford.(1991)
[2] ICRP publ. 103 " Recommendations of the International Commission on Radiological Protection,". Annuals of ICRP Vol.37, Permagon Press Oxford.(2007)
[3] ICRP publ. 74 " Conversion Coefficients for use in Radiological Protection against External Radiation", Annals of the ICRP Vol.26 (1996)
[4] S.Roesler & G.R.Stevenson " Deq99.f-A FLUKA user routine converting fluence into effective dose and ambient dose equivalent ", Technical Note CERN-SC-2006070-RP-TN EDMS No.09389 (2006)
[5] ICRU, "Quantities and Units in radiation protection dosimetry," Report 51 ICRU Publications (1997)
[6] J.Liu et al., "Comparison of design and practices for radiation safety among five synchrotron radiation facilities", Radiation Measurements 41 (2007)
[7] Y.Asano, "Characteristics of radiation safety for synchrotron radiation and X-ray free electron laser facilities", Radiation Dosimetry 146 No.1-3 (2011)
[8] H.A.Baldis, E.M.Campbell, and W.L.Kruer," Handbook of Plasma Physics", Elsevier Science Publisher, (1991)
[9] S.C.Wilks and W.L.Kruer, IEEE J.Quantum Electron 33 (1997)
[10] S.J.Gitmore et al., Fast ions and hot electrons in the laser-plasma interaction. Phy.Fluids 29, (1986)
[11] W.P.Swanson, "Radiological Safety Aspects of the operation of electron linear accelerators", IAEA technical Reports No.188 (1979)
[12] H.C.Dehne et al., Nuclear Instruments and Methods 116 p345 (1974)
[13] G.F.Knoll," Radiation Detection and Measurements,3rd edition", John Willy & Sons,Inc (New York ISBN 0-471-07336-5 (1999)
[14] H.Yasuda & T.Ishida," Time resolved photoluminescence from a phosphate Glass irradiated with heavy ions and gamma rays", Health Physics 84, No.3 (2003)
[15] A.Klett, A.Leushner, " A Pulsed neutron Monitor", ,IEEE 2007 Nuclear Science Symposium and Medical Imaging Conference, Honolulu USA (2007)
[16] F. d'Errico, "Radiation dosimetry and spectrometry with superheated emulsions", Nuclear Instr.& Methods B184 (2001)
[17] H.Hirayama, Y.Namito, A.F.Bielajew, S.J.Wilderman, and W.R.Nelson.," The EGS5 Code system", SLAC-R-730, KEK-Report 2005-8 (2005)
[18] F.Salvat, J.M.Fernandes-Varea,E.Acosta, and J.Sempau,"PENELOPE, A code system for Monte Carlo Simulation of Electron and Photon Transport", NEA/NSC/DOC (2001)19 ISBN:92-64-18475-9
[19] D.B.Pelowitz et al., "MCNPX 2.7.0 Extensions", LA-UR-11-02295 (2011)
[20] A.Ferrari, P.R.Sala, A.Fasso, and J.Ranft," FLUKA; a multi-particle transport code",CERN 2005-10(2005), INFN/TC_05/11, SLAC-R-773
[21] N.V.Mokhov & S.T.Striganov," MARS15 Overview", Fermilab-conf-07/008-AD (2007)
[22] S.Agostinelli et al., GEANT4 – a simulation tool kit", Nuclear Instruments & Methods A 506 250 (2003)
[23] K.Niita et al., " PHITS; Particle and Heavy Ion Transport code System V2.23 JAEA-Data/Code 2010-022 (2010)

[24] Y.Asano and N.Sasamoto,"Development of shielding design code for synchrotron radiation beamline", Radiation Physics & Chemistry 44(1/2) 133 (1994)
[25] T.Tanaka,"FEL simulation code for undulator performance emission" Int.Proceeding FEL2004 Trieste, (2004)
[26] Y.Hayashi,et al.," Estimation of photon dose generated by a short pulse high power laser", Radiation Protection Dosimetry 121 (2) 99 (2006)
[27] W.R.Nelson and T.M.Jenkins," The SHIELD11 Computer code", SLAC-Report 737 (2005)
[28] T.M.Jenkins,"Neutron and photon measurements through concrete from a 15 GeV electron beam on target-Comparison with models and calculations", Nucl.Instr.& Methods 159 265 (1979)
[29] H.Hirayama, and S.Ban," Neutron dose equivalent outside the lateral shielding of an electron linear accelerator oprating at 0.85GeV", Health Physics 56 6 (1989)
[30] A.Ferrari, M.pellicioni, and P.R.Sala, "Estimation of fluence rate and absorbed dose rate due to gas bremsstrahlung from electron storage rins", Nucl. Instrum. Methods B83 518 (1993)
[31] J.C.Liu, W.R. Nelson, and K.R.Kase, "Gas Bremsstrahlung and Associated Photo-neutron Shielding Calculations for Electron Storage Ring, SLAC-Pub. 6532 (1994)
[32] K.Tesch, "Attenuation of the PHOTON Dose in Labyrinths and Duct at Accelerators", Radiation Protection Dosimetry 20 169 (1987)
[33] K.Tesch " The Attenuation of the Neutron Dose Equivalent in a Labyrinth through an Accelerator Shield", Particle Accelerators 12 169 (1982)
[34] T.Shintake et al., " Status of SCSS; SPRING-8 Compact SASE Source Project", Proc. 8th European Particle Accelerator Conf. Paris 2002, European Organization for Nuclear Research (2002)
[35] Y.Asano, T.Itoga, and X.Marechal," Radiation Shielding Aspects of the SCSS prototype XFEL facility", Nuclear Technology 168 (2009)
[36] G.Lambert et al., "Injection of harmonics generated in gas in a Free-Electron Laser providing intense and coherent extreme-ultraviolet light", Nature Phys., 4 296 (2008)

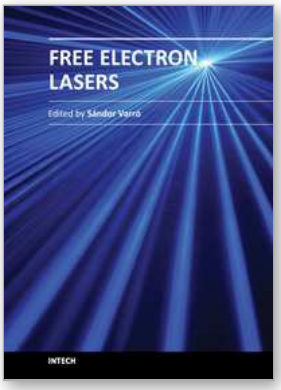

Free Electron Lasers
Edited by Dr. Sandor Varro

ISBN 978-953-51-0279-3
Hard cover, 250 pages
Publisher InTech
Published online 14, March, 2012
Published in print edition March, 2012

Free Electron Lasers consists of 10 chapters, which refer to fundamentals and design of various free electron laser systems, from the infrared to the xuv wavelength regimes. In addition to making a comparison with conventional lasers, a couple of special topics concerning near-field and cavity electrodynamics, compact and table-top arrangements and strong radiation induced exotic states of matter are analyzed as well. The control and diagnostics of such devices and radiation safety issues are also discussed. Free Electron Lasers provides a selection of research results on these special sources of radiation, concerning basic principles, applications and some interesting new ideas of current interest.

InTech Europe
University Campus STeP Ri
Slavka Krautzeka 83/A
51000 Rijeka, Croatia
Phone: +385 (51) 770 447
Fax: +385 (51) 686 166
www.intechopen.com

InTech China
Unit 405, Office Block, Hotel Equatorial Shanghai
No.65, Yan An Road (West), Shanghai, 200040, China
中国上海市延安西路65号上海国际贵都大饭店办公楼405单元
Phone: +86-21-62489820
Fax: +86-21-62489821